Title: Increased rates of hybridization in swordtail fish are associated with water pollution

Authors:

Benjamin M Moran[1,2,3], Wilson F Ramírez-Duarte[2,4,5], Daniel L Powell[1,2,6], Terrance TL Yang[1], Theresa R Gunn[1,2], Gaston I Jofre-Rodríguez[2,7], Cheyenne Y Payne[8,9], Erik NK Iverson[10], Gabriel E Preising[1,2], Shreya M Banerjee[3], Alexandra E Donny[1,11], Rhea Sood[1], John J Baczenas[1], Gabriela María Vázquez Adame[2], Carla Gutiérrez-Rodríguez[12], Chelsea M Rochman[4], Molly Schumer[1,2,13]*, Gil G Rosenthal[2,14]*

Affiliations:

[1]Department of Biology, Stanford University

[2]Centro de Investigaciones Científicas de las Huastecas "Aguazarca", A.C.

[3] Present Address: Department of Evolution and Ecology, University of California at Davis

[4]Department of Ecology & Evolutionary Biology, University of Toronto

[5]Present Address: Department of Environmental & Physical Sciences, Concordia University of Edmonton

[6] Department of Biological Sciences, Louisiana State University

[7]Department of Biology, Virginia Commonwealth University

[8]Department of Ecology and Evolutionary Biology, University of California, Santa Cruz

[9]Southwest Fisheries Science Center, National Marine Fisheries Service, National Oceanic and Atmospheric Administration

[10]Department of Integrative Biology, University of Texas at Austin

[11]Department of Genome Sciences, University of Washington

[12] Red de Biología Evolutiva, Instituto de Ecología A.C

[13]Freeman Hrabowski Fellow, Howard Hughes Medical Institute

[14]Dipartimento di Biologia, Università di Padova

*co-supervised this work

Running Head: Anthropogenic hybridization in swordtails

Keywords: hybridization, hybrid populations, anthropogenic change, water pollution, mate choice, freshwater fish, swordtail fish

Abstract

Biodiversity loss can occur when disturbance compromises the reproductive barriers between species, causing them to collapse into a single population through hybridization. Recent research has documented an increasing number of cases where anthropogenic environmental disturbance is associated with new hybrid populations, but few studies have been able to quantitatively compare potential environmental drivers and test possible mechanisms connecting interspecific hybridization to anthropogenic disturbance. Here, we combine genomic and chemical surveys to explore the loss of reproductive isolation between the sister species *Xiphophorus malinche* and *X. birchmanni*, fishes whose riverine habitat in the Sierra Madre Oriental of Mexico is increasingly impacted by human-mediated disturbance. By sequencing whole genomes of thousands of fish, we characterize the landscape of hybridization between these species in four distinct rivers. Ancestry structure varied dramatically across rivers, ranging from stable coexistence to clinal hybrid zones, hinting that dynamics of hybridization in this system may be environmentally dependent. In one river, we discovered that a sudden transition in patterns of hybridization coincides with its passage through an urbanized area, with upstream sites showing distinct ancestry clusters and downstream sites showing a swarm of hybrids with variable ancestry. Water chemistry measurements show that water quality changes significantly over this area, including in parameters known to disrupt fish olfaction and mating. We hypothesize that the hybrid swarm downstream of the town is driven by disruption of olfaction that impacts mating preferences. We test this by sequencing mothers and embryos from sites downstream of the urbanized area, and find reduced assortative mating, in contrast to strong assortative mating in sites upstream. We document alterations of the olfactory epithelium at the

same site which are consistent with chemical irritation. Taken together, our work illuminates the mechanisms linking anthropogenic disturbance to the breakdown of reproductive isolation in hybridizing species.

Introduction

Biologists have known for decades that hybridization can be associated with environmental disturbance (1, 2). Disturbed habitats bring together species which do not coexist under other circumstances, create novels environments which may provide better habitat for hybrids than those of undisturbed habitats, and may alter the interactions between species that previously coexisted without interbreeding (1–3). While natural changes to the environment may have been the major source of disturbance historically, human impacts on the environment (e.g. land conversion, pollution, resource extraction) may play an analogous role in promoting hybridization in recent decades (4–7). As human impacts on the environment become ubiquitous (8), the connection between disturbance and hybridization would suggest the number of hybrid zones should be growing as well. In fact, the rate of hybridization appears to be increasing across a range of taxa, largely due to anthropogenic impacts on the environment (3).

In investigating the connection between disturbance and hybridization, early researchers hypothesized that hybrids appear in disturbed areas because the barriers that prevent mating between closely related species can break down in novel environmental contexts (1). Such "premating" barriers often arise early in the divergence of two lineages (9, 10) and thus may be especially important in the origin and preservation of biodiversity (11–13). The link between disturbance and hybridization has been supported by empirical work that shows that premating barriers, such as a behavioral preference to mate assortatively by species, are highly context-dependent (14–18), sensitive to environmental conditions (19, 20), and may disappear in the face of disturbance that impacts mechanisms of mate discrimination (6, 21, 22). Human modification

89 of the environment can interfere with mechanisms used to identify conspecifics, either by
90 directly affecting signal production or transmission or by abolishing conspecific preferences in
91 the choosy sex (6, 23, 24). In aquatic species, in particular, a variety of chemical pollutants have
92 been shown to ablate or even reverse conspecific mate preferences (6, 23–27).

93 If assortative mating is a major reproductive barrier between species (or genetically
94 distinct subpopulations), weakening this barrier can lead to a sudden collapse of population
95 structure and phenotypic divergence (28–32), often referred to as a "hybrid swarm". Since mate
96 discrimination is typically weaker in hybrids than in parental species (21), this can lead to
97 irreversible phenotypic and genetic homogenization through hybridization (i.e. "speciation
98 reversal" or "genetic swamping"). Although hybridization may sometimes lead to the formation
99 of new species (33), hybrid speciation without a change in chromosome number appears to be
100 relatively rare (34), and the immediate consequence of the formation of hybrid swarms is more
101 often the loss of genetic differentiation and functional biodiversity (7, 35). Moreover, early-
102 generation hybrids often experience inviability or sterility due to intrinsic hybrid
103 incompatibilities (36, 37) between the parental genomes (although we note that hybridization can
104 also facilitate adaptation; (38, 39)). Thus, in addition to its direct effects of homogenizing
105 divergent species, hybridization may also decrease overall population size and fecundity.

106 The swordtail fishes of the genus *Xiphophorus* provide a compelling system in which to
107 study the barriers to gene flow in natural populations and their breakdown following
108 anthropogenic disturbance. As model systems for hybridization and mate choice, *Xiphophorus*
109 species have been subject to numerous studies showing that mating preferences can be altered by
110 environmental and social context (15, 16, 21, 23). Swordtails are found in the eastern slopes of
111 the Sierra Madre Oriental and Gulf coastal plain of Mexico, a region experiencing growing

human population density and agricultural land conversion since the 20th century (40, 41). This change in land cover has impacted water quality in the region, while also threatening the area's exceptional biodiversity (42, 43). In particular, the sister species *X. malinche* and *X. birchmanni* overlap in the montane rivers of Hidalgo, Mexico, where steep slopes create frequent barriers to migration (waterfalls, cascades, and subterranean river reaches) and coincide with dramatic ecological variation over short geographic distances. *X. malinche* occupy cool headwater streams while *X. birchmanni* are found in warmer lower-elevation rivers, creating the potential for ecological selection against hybrids (44, 45). In addition, early-generation hybrids between these species suffer from severe genetic incompatibilities (46–48). However, some hybrids are viable and fertile, and natural hybrid zones can be found in multiple independent stream reaches (49, 50). Researchers first reported hybridization between *X. malinche* and *X. birchmanni* in 1997, whereas hybrids were not detected when sampling this site a decade earlier (51, 52). Meanwhile, the period of 1980-1995 saw a 37% increase in population in the state of Hidalgo (53). Independent genetic approaches have estimated that these hybrid zones are on the order of ~100 generations old (54), consistent with hybridization beginning in the late 1900s. The recent onset of hybridization begs the question of what triggered it, and whether it was tied to the concurrent socio-ecological transformation of the region.

Though we lack ecological data from these rivers prior to the beginning of hybridization, spatial patterns in present day populations may provide insights into the drivers of hybridization. The genetic structure in most hybrid populations is best described as a hybrid swarm lacking population structure (49). One exception to this pattern among described populations is a river reach just upstream of the town of Calnali, Hidalgo. There, genetic studies have described two subpopulations of *malinche*-like and *birchmanni*-like admixed fish that exist in sympatry (Fig. 1;

(55). Sequencing over multiple years showed that this bimodal population structure has been stable over time, and is best explained by strong assortative mating between individuals of the same ancestry group (55). However, recent sampling of a population downstream in the same river showed that population structure disappears just downstream of the town of Calnali (46), raising the possibility that assortative mating breaks down after exposure to a point pollution source.

Here, we use whole-genome sequencing of 2620 fish and comprehensive surveys of water chemistry to study the relationship between environmental conditions and patterns of hybridization across multiple *X. malinche* × *X. birchmanni* hybrid zones in Hidalgo, Mexico. We survey hybrid ancestry in four rivers and compare hybrid population structure across demographically independent hybrid zones. We find that assortative mating between ancestry clusters in the Río Calnali breaks down at the precise point where anthropogenic inputs drastically change water chemistry, leading to a sudden change in population structure. Based on comprehensive water chemistry measurements, we identify multiple pollutants which spike at the point of population structure collapse. We find that this pattern of population structure collapse is unique among rivers surveyed, with other river systems showing little change in population structure over broad geographic distances. Using land use classification of satellite imagery, we confirm that these changes in water chemistry downstream on the Río Calnali are coupled with a uniquely high density of built infrastructure in close proximity to the river. Given the known importance of olfactory communication in swordtail mate choice, we test for evidence of damage to olfactory rosettes as a result of natural or lab exposure to pollutants. We find evidence of greater histological damage in polluted sites compared to less disturbed sites. This work thus

157 establishes a quantitative link between environment, phenotype, and genomics in an

158 anthropogenic hybrid zone, deepening our understanding of human impacts on biodiversity.

Materials and Methods

Study area and sample collection

We collected fin clips from 44 sites across four stream basins which together compose the Río Atlapexco drainage of Hidalgo, Mexico (see Table S1 for full list with GPS coordinates) for low-coverage whole genome sequencing. Fish were collected using baited minnow traps and anesthetized in a buffered solution of 100 mg/mL MS-222 dissolved in stream water (Stanford APLAC protocol #33071). Fish were allowed to recover after fin clips were collected, then were returned to the pool from which they had been sampled. Tissue was stored in 95% ethanol for DNA extraction. A subset of female fish from the Calnali Low population (Fig. 1) were euthanized and stored with their embryos in 95% ethanol for analysis of assortative mating (see below). In addition, 30 fish each from the Aguazarca and Calnali Low populations were decapitated following euthanasia, with whole heads preserved in 10% neutral buffered formalin for olfactory histology (see below).

DNA extraction and coverage whole-genome sequencing

DNA was extracted from preserved fin clips using the Agilent DNAdvance extraction kit (Beckman Coulter, Brea, California). The protocol for extractions followed the manufacturer's instructions for the tissue extraction version of the protocol except that we used half-reactions. Extracted DNA was quantified on a BioTek Cytation5 (Agilent, Santa Clara, CA) microplate reader, and diluted to 10 ng/µl for library preparation. We used a previously described

182 tagmentation-based protocol to prepare DNA for sequencing (44). Libraries were dual-indexed
183 via amplification (12 PCR cycles) and purified using 18% SPRI beads. Libraries were quantified
184 on a Qubit Fluorometer (Thermo Scientific, Wilmington, DE) and library size distribution was
185 visualized on an Agilent 4200 Tapestation (Agilent, Santa Clara, CA). Libraries were sequenced
186 at Weill Cornell Medical College, Harvard Bauer Core, and Admera Health Services (South
187 Plainfield, NJ).
188
189 *Local ancestry inference*
190
191 Hybrids between *X. birchmanni* and *X. malinche* harbor ancestry from both species that
192 varies locally along the genome and globally between individuals and populations. We used an
193 approach developed by our group for accurate local ancestry inference in *X. malinche* × *X.*
194 *birchmanni* hybrids that relies on a hidden Markov model and known ancestry informative sites
195 that distinguish *X. birchmanni* and *X. malinche* to infer local ancestry (*ancestryinfer*; (56)). Both
196 simulation studies (56) and analyses of populations of known ancestry have indicated that this
197 approach has a low error rate (~0.1% per ancestry informative site (47, 57)). Likewise, inference
198 of local ancestry is robust to a number of technical challenges including parameter
199 misspecification (56).
200 We inferred local ancestry using *ancestryinfer* from whole genome sequence data for all
201 individuals for which we collected more than 300,000 reads from the sequencing approach
202 described above. This coverage cutoff was based on previous simulation studies (56) and
203 resulted in 12 to 702 individuals per site post-filtering (median 32; Table S1). *Ancestryinfer*
204 outputs posterior probabilities of ancestry for all informative sites along the genome. In the case

of *X. malinche* × *X. birchmanni* hybrids, this results in estimates of ancestry at 729,167 ancestry informative sites across 24 chromosomes. Since we were primarily interested in accurately estimating global admixture proportion for individuals along a spatial cline, we converted posterior probabilities to 'hard calls' using a threshold of 0.9. For example, if an individual had greater than 0.9 posterior probability for *X. malinche* ancestry, we converted that site to an *X. malinche* state. If a site did not have a posterior probability ≥0.9 for any ancestry state, we converted the site to missing data.

We used these hard calls to estimate the proportion of the genome derived from each parental species. We estimated this proportion using two approaches. First, we calculated the ratio of the number of alleles called for the *X. malinche* state out of the total number of alleles called (treating heterozygous sites as 1 allele for each parental species). We also used a spatially aware approach, given that there is variation in the distance between ancestry informative sites. To do so, we calculated the proportion of the genome covered by high-confidence *X. malinche* or *X. birchmanni* ancestry tracts, excluding regions that were not confidently called from the denominator. In practice, this approach generated nearly identical results (Supp. Info 1; Fig. S1).

With these results in hand, we visualized the distribution of admixture proportion in populations along the Río Calnali, Río Pochula, Río Huazalingo, and Río Conzintla (Fig. 2). As previous results had indicated the presence of bimodal ancestry structure in upstream populations of the Río Calnali, we also calculated Hartigan's dip statistic (58), which quantifies departures from a unimodal distribution, on samples from each collection site. Since we used this test across many sites, we applied a Bonferroni correction for the number of tests. Samples were collected between 2006 and 2024, with the highest sampling density between 2014 and 2022 (Table S2).

Given the broad time period over which samples were collected, we also evaluated whether ancestry structure was stable at a given site across the study period (Supp. Info 2; Fig. S2; (55).

Water chemistry surveys

We chose a subset of 32 sampling sites that captured the full range of variation in ancestry structure present in each river and collected multimodal water quality measurements from these sites between February 2022 and September 2024 (Fig. 1). Due to changes in equipment availability over time, sample sizes for individual water quality measurements varied between 0 and 13 per location and measure; for all measures and sample sizes per location, see Table S3. We measured temperature, conductivity, dissolved oxygen, and fluorescent dissolved organic matter (fDOM) using YSI EXO 2 and EXO 1s multiparameter sondes (Xylem Inc.). Turbidity was measured in nephelometric turbidity units (NTUs) with an Orion AQ4500 Turbidity Meter (Thermo Fisher). Using a YSI 9500 photometer, we applied colorimetric assays to measure pH, total alkalinity, total hardness, calcium hardness, and concentrations of sulfate, sulfite, sulfide, phosphate, ammonia, nitrite, and nitrate. Sonde measurements, turbidity measurement, and colorimetry tests were performed at the site of sampling to ensure the accurate measurement of unstable chemicals, while further measurements were performed on collected water samples. For measurements of dissolved organic carbon (DOC) and total nitrogen, we stored samples in glass vials capped with PTFE/silicone septa, which were combusted at 500 °C for 1 hour and rinsed ten times with ultrapure water (Milli-Q® Merck) prior to sample collection. Water samples were processed on-site by syringe-filtering through a 0.45 μm polyethersulfone

(PES) membrane, acidifying to pH 2-3 using concentrated hydrochloric acid, and capping with no air bubbles remaining in the vial. DOC and N measurements were carried out on a Shimadzu TOC-L analyzer using the TC/IC and TN protocols, respectively, at the Environmental Engineering Laboratory of the National Autonomous University of Mexico (UNAM) and the Environmental Measurements Facility at Stanford University. Total and dissolved metals were measured from samples collected in 50 mL Falcon tubes triple-rinsed with sample water, with samples for dissolved metals filtered through 0.45 μm PES and all samples acidified to a pH of ~2 using trace metal grade nitric acid. Inductively coupled plasma mass spectrometry (ICP-MS) detection of 39 ions was carried out following a modified version of the APHA3030B/6020A methods by ALS Environmental (Waterloo, ON; see Table S4 for full list of ions and QA/QC). Given that many metals in the filtered samples were below the lower detection limits of ICP-MS, we used ICP-MS measurements of total concentration from unfiltered samples in all downstream statistical analyses.

Geospatial Analyses

To complement our measurements of water chemistry, we measured land use in each river catchment as a proxy for anthropogenic disturbance. Briefly, we used Google Earth Engine to access Sentinel-2 multispectral imagery from the month of May in the years 2020-2023 (59), removed images with > 20% cloud cover, masked pixels flagged as clouds, then took the median intensity for each band and pixel to construct a composite image with bands 11 (1610 nm, short-wave infrared, 20 m^2 resolution), 8 (842 nm, near-infrared, 10 m^2), and 2 (490 nm, blue, 10 m^2). This spectral combination provides better contrast between built infrastructure, herbaceous, and

woody vegetation than the visible spectrum (60). All further analyses were performed in ArcGIS Pro (version 3.3.1) with the Spatial Analyst and Image Analyst extensions. We segmented the three-band raster file using the Segmentation tool, with a spectral detail of 18, a spatial detail of 19, and a minimum size per object of 20 pixels. Next, we selected four land use types for classification: water, forest (continuous tree cover, excluding plantation-style agriculture), non-forest vegetation (grassland, pasture, or cultivated crops, including plantation-style orchard), and developed land (buildings, mines, and roads). We included water surfaces (primarily to prevent their misclassification as other land use types), forest as the primary undisturbed land cover in the area, and non-forest vegetation as an additional form of human disturbance beyond hardened infrastructure. Using 3 m^2-resolution imagery of the study area in March 2022 downloaded from Planet Labs (61), we identified 60 polygons of each land class to serve as training samples. Given the short time frame between the capture of our Sentinel and Planet Labs image sets, we assumed that there would be negligible change in the proportion of land classes. We then used the Classification tool to perform object-based land use classification using a support vector machine algorithm with maximum 500 samples per class. We visually inspected the resulting classification for pixels misclassified as developed land, and removed these pixels from the dataset prior to further analyses (0.8% of all pixels).

To delineate catchments for each site, we downloaded a digital elevation model (DEM) of the state of Hidalgo with 15 m^2 resolution from the Mexican National Institute for Statistics and Geography (62). Starting with this DEM, we calculated flow direction and flow accumulation, snapped each site to the nearest pour point pixel, and calculated the land area which drained into the river upstream of a given site (Fig. S3), using the Flow Direction, Flow Accumulation, Snap Pour Points, and Watershed tools, respectively. To identify the land area with greatest potential

for runoff into waterways (i.e. greatest influence on water chemistry), we used the Raster Calculator tool. We converted all cells which received flow from at least 3000 uphill cells into a polyline object representing the relevant waterways in our study area (Fig. S3). We then used the Buffer tool to identify the land area within 500 m, 100 m, and 50 m of these waterways, and used the Clip Raster tool to identify the subset of classified land use pixels within each of these buffers. Using the Zonal Histogram tool, we summed the pixel counts of each land use category in each site's subcatchment, then calculated the proportion of the total pixels per subcatchment composed of each land use type. Finally, we calculated cumulative land use within a site's watershed by summing the land use categories within its own site-specific subcatchment and within the subcatchments of all upstream sites.

Statistical analysis of environmental data

We explored overall differences in water chemistry between sites and drainages using Principal Component Analysis (PCA). Given differing sample sizes of ICP-MS measurement relative to other measures, we conducted two separate PCAs, one for ICP-MS metals measurement (n = 66 measurements) and one for all other data (n = 58). For water chemistry parameters other than metals, we included only measurements which were consistently collected throughout the length of the field study, including dissolved oxygen (mg/L), fDOM (quinine sulfate units), conductivity (µS/cm), total hardness (mg/L $CaCO_3$ equivalent), total alkalinity (mg/L $CaCO_3$ equivalent), pH, nitrite (mg/L N), ammonia (mg/L N), phosphate (mg/L PO_4), sulfate (mg/L SO_4), and turbidity (NTU). Of the 39 ions measured in the metals measurements, we retained 30 which had more than one measurement above the lower detection limits of ICP-

MS. For the purposes of this analysis, metals measurements below the detection limit were set to halfway between zero and the lower detection limit. For example, for cadmium, the detection limit was 5 ng/L and we set values below the detection limit to 2.5 ng/L. While this approach has some limitations (63, 64) compared to alternative approaches using imputation (65), we could not apply imputation approaches to our data given the possibility of systematic differences in concentrations of many of the metals between rivers. However, we explored the potential impacts of this analysis choice on our conclusions by repeating PCAs with the measurements below the detection limit set to the detection limit or zero, and found our results were qualitatively unchanged (Fig. S4).

We also used the PCA analysis to qualitatively compare patterns within and across rivers and identify chemicals of interest for further statistical analysis. Specifically, we chose chemicals which had negative loadings on both PC1 and PC2 in either the non-metal or metal PCA because we found that this approach clearly separated sites downstream on the Río Calnali from the others (Fig. 4). From this set of parameters, we next investigated which had evidence for affecting fish neurobiology, olfaction, or mate choice in the literature. These parameters included DOM (23), turbidity (66), nitrite (67), ammonia (68, 69), copper (70, 71), lead (72), cadmium (73, 74), zinc (75), and aluminum (76). In the analysis of ICP-MS metals data, where the effects of samples below the detection limit prevented the use of parametric tests, we used Kruskal-Wallis tests to identify differences in concentration within and between drainages. For all other variables, we used ANOVA and Tukey's HSD tests to confirm differences between the downstream Calnali sites and the other groups, testing for differences in the log-transformed response variables as a function of drainage, sampling month, and their interaction. We also used

the same approach to explore differences in water chemistry between watersheds (Supp. Info 3; Fig. S5-6) and over different years across the sampling period (Supp. Info 4; Fig. S7-9).

Finally, we tested whether broad-scale variation in water chemistry was associated with variation in land use along the rivers. We created a combined dataset of all parameters described above, calculated the site-wise average of each water quality parameter across all measurements, and then constructed a PCA (n = 30 sites). We found that the variation in the PCA largely mirrored our prior analyses on subsets of the data discussed above (Fig. S10). We then conducted two separate linear regressions with the top two principal components of water chemistry variation as response variables, each as a function of five explanatory variables: the site-specific and cumulative proportion of developed land upstream of the site, the site-specific and cumulative proportion of non-forest vegetation upstream of the site, and the total watershed area. We repeated our analyses considering only land use within 50 m of the closest point of the river, and also evaluated the effects of using different approaches to account for detection limits in the ICP-MS measurements (setting measurements to the detection limit, zero, or a random uniform variable drawn between zero and the detection limit; Table S10-12).

Analysis of ancestry assortative mating in Calnali Low

Previous work has shown that the vast majority of individuals above the town of Calnali on the Río Calnali fall into one of two ancestry clusters: a *X. birchmanni* biased cluster that derived ~75% of its genome from *X. birchmanni* and a *X. malinche* biased cluster that derives >90% of its genome from *X. malinche*. These distinct ancestry clusters are maintained by strong ancestry-assortative mating (55). In this study, we identify the Calnali Low population as one of

364 the first sampling sites where this genetic structure breaks down along the Río Calnali. As a
365 result, we were interested in evaluating levels of ancestry assortative mating in this population.
366 To do so, we analyzed mother-embryo samples from the Calnali Low population,
367 including previously published samples collected in 2020 (47), as well as newly sequenced
368 samples from a 2017 collection. Because swordtails are livebearing fish which exhibit multiple
369 paternity, when we collect pregnant *X. malinche* × *X. birchmanni* females we also collect ~10
370 offspring from an average of three fathers. Although we cannot directly assay the paternal
371 genotypes, since the maternal genotype can be directly determined, we can use the ancestry of
372 the offspring to infer the ancestry of the male the female mated with, since offspring will inherit
373 approximately 50% of their genome from each parent. Thus, the difference between the mother's
374 genome-wide ancestry and the genome-wide ancestry of her offspring is a useful proxy for
375 paternal ancestry.
376 We have previously used this approach to quantify ancestry assortative mating in
377 upstream populations on the Río Calnali (55), and repeat this approach here. Specifically, we ask
378 about the observed difference between maternal and offspring ancestry genome-wide in the
379 Calnali Low population, compared to expectations under a scenario where females mate at
380 random with respect to male ancestry. To generate a distribution of offspring ancestry expected
381 under no assortative mating, we performed simulations. For each focal female in our dataset (n =
382 74), we randomly sampled a mate from our full dataset of 702 adults from the Calnali Low
383 population. Next, we calculated the mean of the maternal and simulated paternal ancestry. We
384 added noise to this average ancestry by sampling from a random normal distribution with the
385 mean set to the variance in admixture proportion among full siblings observed in our data (Supp.
386 Info 6). We repeated this procedure until we had simulated offspring for all of the focal females.

387 We generated 1,000 replicate simulations and compared the observed and simulated differences
388 in mother-offspring admixture proportions in the Calnali Low population.
389
390 *Inferring the strength of assortative mating from observed maternal-offspring ancestry*
391 *distributions*
392
393 We found evidence that the observed mother-offspring ancestry patterns in the Calnali
394 Low population differed subtly from patterns expected if mating were truly random with respect
395 to ancestry (Fig. 5B). However, this difference from random mating was much weaker than
396 observed in upstream populations on the Río Calnali. To quantitatively compare the strength of
397 ancestry-assortative mating consistent with the observed data, we used the same approach we
398 previously used to quantify the strength of ancestry assortative mating in the Aguazarca hybrid
399 population (55).
400 Briefly, we used an approximate Bayesian computation approach to evaluate what levels
401 of ancestry-assortative mating were consistent with our observed data. We drew a probability that
402 a female would accept a mate with an ancestry proportion that differed from hers by more than
403 5% (see Supp. Info 6 for simulations using different thresholds) from a random uniform
404 distribution ranging from 0 (perfect assortative mating) to 1 (random mating). We refer to this
405 value as the strength of assortative mating. For each female we then randomly drew a mate from
406 the population ancestry distribution. If the mate fell within the ancestry threshold, the mate was
407 accepted. If it did not, we used a random binomial weighted by the strength of assortative mating
408 to determine if the mate was accepted. If the mate was rejected, we continued this procedure
409 until the female was matched with a mate, then simulated offspring as described above. This was

410 repeated until all females were matched with a mate. We repeated this simulation procedure for a
411 total of 100,000 simulations.
412 We used a simple rejection sampling approach to select simulations that closely matched
413 the empirical data. For each simulation, we calculated the mean and variance of the difference in
414 ancestry between mothers and their offspring. If both summary statistics fell within 5% of the
415 observed value for the Calnali Low population (mean 6.6%, variance 0.46%), we accepted the
416 simulation. This allows us to estimate the range of values of assortative mating consistent with
417 our data. We plotted the posterior distribution of accepted assortative mating strengths and
418 identified the maximum a posteriori (MAP) estimate. We repeated this procedure with other
419 thresholds of ancestry proportion differences (see Supp. Info 6; Fig. S11). To evaluate whether
420 results were affected by our approach in modeling assortative mating, we also explored an
421 alternative approach modelling assortative mating as a continuous beta function (Supp. Info 7;
422 Fig S12).
423
424 *Histology in wild-caught fish*
425
426 Like their relatives (77), *X. malinche* × *birchmanni* hybrids have plate-like olfactory
427 rosettes with beds of sensory epithelia surrounded by ridges of nonsensory tissue (Fig. S13).
428 Sensory epithelial beds contain a combination of ciliated and microvillous olfactory neurons,
429 which collect and transmit chemical information to the olfactory bulb, and ciliated sustentacular
430 cells, which increase flow over the beds to heighten olfactory sensitivity (78, 79). The
431 intervening nonsensory ridges are composed largely of connective tissue and goblet cells, the
432 latter of which are responsible for producing the glycoprotein-based mucus which physically

433 shields the epithelium from irritants (77, 80). Based on reports from the literature (70, 80–83),
434 we quantified the loss of cilia from the sensory epithelial surface and the proliferation of goblet
435 cells in the nonsensory epithelium and treated these two measures as a proxy for olfactory
436 disruption.

437 To understand whether polluted water was directly impacting the sensory periphery of
438 fish in *X. malinche* × *birchmanni* populations, we collected a total of 30 fish each from the
439 Aguazarca and Calnali Low populations in May (n = 10 per site) and September (n = 20) 2022.
440 Fishes were euthanized by MS-222 overdose and decapitation, after which heads were fixed in
441 10% buffered formalin for at least 48 hours. Fixed crania were dissected to remove the gills and
442 lower jaw, decalcified for 8 hours in 1X PBS with 10% formic acid, then dehydrated for 20
443 minutes each in 30%, 50%, and 70% ethanol before long-term storage in 70% ethanol. Samples
444 were submitted to Histo-Tec Laboratories (Hayward, CA) for xylene clearing, paraffin
445 embedding, sectioning, and staining. Horizontal sections were taken at 5 μm intervals with a
446 rotary microtome after removing 75-150 μm of tissue from the dorsal surface, with deeper
447 sectioning needed to reach the olfactory epithelia in larger individuals. One slide per individual
448 was prepared with hematoxylin and eosin (H&E) staining to observe gross morphological
449 changes (i.e. presence/absence of ciliary on olfactory epithelium). Samples from one collection
450 (May 2022) were also subject to Alcian Blue / Periodic Acid-Schiff stain for mucoproteins to
451 identify mucus-producing goblet cells, with eosin as a counterstain. Individuals for whom
452 olfactory rosettes were not present in the Histo-Tec slides (3 from Aguazarca and 1 from Calnali
453 Low for H&E slides, 1 each for AB/PAS slides) were excluded from further analysis.

454 A blinded observer examined the slides at 1000X magnification using oil immersion. The
455 observer defined the bounds of each sensory epithelial bed, and estimated the proportion of the

456 surface area of each bed on which cilia were visible to the nearest 10%. Further, we scanned and
457 imaged each slide at 40x magnification via a Biotek Cytation5 microplate reader, utilizing the in-
458 place ruler on the image to calculate the length of each bed in ImageJ. We normalized ciliated
459 proportions by bed length to calculate the total proportion of the sensory epithelium with visible
460 cilia in each individual, then used a Mann-Whitney *U* test to test for differences in ciliated
461 surface proportion between fish from Aguazarca and Calnali Low. Kolmogorov-Smirnov tests
462 indicated that the ciliated surface proportions were not significantly different between the two
463 sampling months ($P > 0.05$), and that other potentially confounding technical factors (number of
464 sensory beds, individual bed length, and total bed length) also did not differ significantly
465 between the two populations or sampling months ($P > 0.05$). To estimate the density of goblet
466 cells, a blinded observer counted all cells positive for AB/PAS staining within a bed, and we
467 tested for a significant difference between populations in the number of cells per individual,
468 corrected for total rosette length, using Mann-Whitney *U* tests. We also performed chemical
469 treatment trials in laboratory settings to explore whether we could induce similar patterns
470 through short-term chemical exposure (Supp. Info 8; Fig. S14-15).

Results

Population structure across rivers

Ancestry structure varied markedly among the four rivers sampled for this study. One river, the Pochula, showed a relatively smooth cline in ancestry from pure *X. malinche* at high elevations to *X. birchmanni*-like hybrids at lower elevations. The other three rivers varied in the degree of population structure, with at least one site in the Calnali, Huazalingo, and Conzintla showing evidence of significant departures from unimodality based on the distribution of individual ancestry proportions (Fig. 2; Hartigan's Dip Test $P < 0.0001$). Examination of the variation in individual ancestry in these populations supported the presence of two subpopulations with distinct genome-wide ancestry.

Though we identify subpopulations of different ancestry in each river, we infer that the drivers of these patterns differ dramatically. On the Río Huazalingo, the presence of two subpopulations was only detected at a site directly downstream of a waterfall separating pure *X. malinche* from admixed *X. birchmanni*. At this site, pure *X. malinche* individuals were sometimes detected downstream of the waterfall, but this pattern varied between sampling seasons, hinting that the *X. malinche* individuals may not persist in this population (Supp. Info 2; Fig. S2). In the Río Conzintla, we observed sympatry between nearly-pure *X. malinche* and *X. birchmanni*; no recent-generation hybrids were detected at this site. Downstream of these sympatric sites, the *X. malinche* cluster disappears and leaves a single *X. birchmanni* ancestry cluster (Fig. 2; Table S5). The ancestry fraction in this *X. birchmanni* cluster was stable across all sites upstream of a point

where the river passed underground (Kolmogorov-Smirnov Test $P > 0.05$), suggesting that there is little ongoing gene flow between species in this drainage.

By contrast, in the Río Calnali, we observe a dramatic collapse in population structure centered on the town of Calnali (Fig. 2). Sites upstream of the town, spanning 3.15 river kilometers, show strong departure from unimodality in their ancestry distributions ($D = 0.12 – 0.21$, $P < 0.00001$ for all sites; Table S5). *X. malinche*-like and *X. birchmanni*-like subpopulations co-exist in sympatry across these sites, but sites downstream of the town plaza show evidence of a unimodal distribution ($D = 0.01 – 0.07$, $P > 0.18$ across all sites; Table S5) with intermediate mean ancestry and increased variance in individual ancestry proportion. Intriguingly, average *X. malinche* ancestry fraction increased downstream of the town of Calnali (Fig. 2), in contrast to expectations given the geographical distribution of *X. malinche* populations in other rivers. To further investigate this pattern, we collected samples from tributaries flowing into this section of the Calnali, and concluded that migration of individuals with high *X. malinche* ancestry from tributaries into the main river is a plausible explanation for this observed shift in ancestry (Supp. Info 9; Fig. S18).

Land use across drainages

Land use quantification showed that human impact on the Río Calnali watershed was indeed higher than other rivers. The reaches where the river passed through the town of Calnali had the highest proportion of developed land in the study area, with unparalleled levels of urbanization compared to surrounding areas. This increased level of urbanization was centered on the location of genetic population structure collapse in the town of Calnali (Fig. 3). When

calculating the cumulative watershed land input of a given point, the downstream sites on the Río Calnali had the highest proportions of developed land in the study area (Fig 3B), especially when considering land within a short distance of the river (Fig. 3E; Fig. S19H). In contrast, we observed no similar association of cleared land (vegetation, with the exclusion of forest) with population structure on the Río Calnali for any given stream reach or at the watershed scale. When compared to other rivers, though, the Río Calnali did show higher levels of cumulative cleared area within a short distance of the river (Fig. S20F, S20H). Overall, our findings suggest that disruption of forest is ubiquitous throughout the Atlapexco drainage, including in rivers with low levels of hybridization. By contrast, the level of built infrastructure is especially high in the Calnali subcatchment.

Water chemistry variation aligns with breakdown of population structure

Water chemistry varied dramatically both between rivers and between sites on the same river. Principal component analysis demonstrated that the majority of variation in water quality could be summarized by two axes: one that largely separates the sites by river (PC1), and another separating the sites upstream of the town of Calnali from the other rivers and those downstream of Calnali (PC2; Fig. 4). Sites downstream of the town of Calnali were associated with increased dissolved organic matter, turbidity, ammonia, and nitrite, as well as reduced dissolved oxygen, all consistent with increased anthropogenic impacts (Fig. 4). Statistical tests indicated that levels of turbidity, DOM, nitrite, and ammonia were all significantly elevated in the sites downstream on the Río Calnali relative to the upstream sites and to other rivers (Fig. 4, Supp. Fig S16; Table S7-

S8). Across rivers, there was variation in total conductivity, alkalinity, hardness, and pH, with sites in the Río Conzintla having the highest values of each of these metrics and sites along the Río Calnali having the lowest (Fig. 4; Fig. S22).

High concentrations of a range of metals have been previously linked to breakdowns in neurological or olfactory function in fish (27). Given the potential relationship between such breakdown and changes in ancestry assortative mating, we were interested in whether any metals were elevated in waters downstream of the town of Calnali, but not in other sites or across rivers. A principal component analysis showed that concentrations of many dissolved ions, measured by ICP-MS, were highest in the Conzintla and lowest in the Calnali (Fig. 4; Fig. S24). However, the transition from the sites upstream to downstream of the town of Calnali was also associated with a dramatic increase in the concentration of numerous ions, especially major industrial metals (e.g. iron, aluminum, copper, lead, manganese; Fig. 4). Multiple metals significantly increased in concentration downstream of the town of Calnali when individually tested, including copper, lead, cadmium, aluminum, and zinc (Kruskal Wallis $P < 0.001$; Fig. 4; Fig. S23). On the other hand, other ions with known effects on fish neurobiology or olfaction showed similar or higher concentration in the Conzintla than in the Calnali downstream sites, including manganese, arsenic, and calcium (Supp. Info 3; Fig. S24). Though we lack sufficient sampling to formally analyze these effects, we also found some evidence for temporal fluctuations in metal concentrations across rivers (Supp. Info 4; Fig. S7-9).

Finally, to quantify whether changes in water chemistry parameters were connected to land use change, we independently modelled the first two principal components of water chemistry variation as a function of both the site-wise and cumulative area of developed and cleared land, accounting for cumulative watershed area as a covariate. We found that PC1 was

strongly correlated with the cumulative area of both developed ($P < 0.001$) and cleared land ($P < 0.001$), while PC2 was strongly associated with the proportion of developed ($P = 0.032$) and cleared ($P = 0.002$) land immediately upstream of a site. We found that limiting our analysis to land in close proximity to the river increased the relative importance of developed land as a predictor of both PC1 and PC2. In general, our results were not sensitive to various approaches to analyzing ICP-MS values below the detection limit (Table S9-S12). We thus concluded that the proportion of built infrastructure in the watershed was the strongest predictor of water chemistry variation, with the most dramatic impacts in the Río Calnali downstream of the town of Calnali.

Strength of ancestry-assortative mating in the Calnali Low and Aguazarca hybrid populations

In the upstream hybrid population on the Río Calnali, the Aguazarca population, we previously documented bimodal ancestry structure (55). This strong ancestry structure appears to be driven by nearly complete assortative mating by ancestry type in this population (55). By contrast, the Calnali Low population does not show evidence of bimodal ancestry structure, although variance in ancestry is high, potentially indicative of recent admixture between the *X. birchmanni* and *X. malinche* ancestry clusters (Fig. 2). We used paired mother-embryo sequencing to evaluate whether mating patterns differed from expectations under random mating with respect to ancestry. Intriguingly, despite the dramatic breakdown in population structure, we found that mothers and offspring were less different in ancestry than expected under simulations of truly random mating (Fig. 5A). However, the average difference in mother-offspring ancestry was significantly greater in the Calnali Low hybrid population (0.0655) than the prior estimate

585 from the Aguazarca population (0.022; $P < 0.0001$ by simulation), hinting that assortative mating
586 by ancestry is substantially weaker in the Calnali Low hybrid population.
587 Given this result, we sought to quantify the strength of ancestry assortative mating in the
588 Calnali Low population and compare it to that observed in the upstream Aguazarca population.
589 We used an approximate Bayesian computation approach to ask what strength of ancestry
590 assortative mating was consistent with the average difference in ancestry between mothers and
591 offspring that we observe in the Calnali Low hybrid population (see Methods). Based on
592 accepted simulations, we recovered a well-resolved posterior distribution of the strength of
593 ancestry assortative mating, and estimated the maximum a posteriori (MAP) to be 0.65 (Fig. 5B).
594 This is substantially weaker than estimates from the Aguazarca population, in which estimates of
595 assortative mating by ancestry approach 1 (55). Thus, our results suggest that weaker assortative
596 mating contributes to the breakdown in population structure in the Calnali Low hybrid
597 population.
598
599 *Olfactory disruption as a function of water chemistry*
600
601 Changes in olfaction can affect mate discrimination in *Xiphophorus (23, 26)*, and we
602 found that fish in heavily impacted sites on the Río Calnali have been exposed to high levels of a
603 range of compounds that may impact olfactory function. We therefore evaluated evidence for
604 physical damage of the olfactory rosettes of wild caught fish from different sites on the Río
605 Calnali, and found that fish collected from the upstream site, Aguazarca, and the downstream
606 site, Calnali Low, showed significant changes in olfactory morphology. H&E staining allowed us
607 to observe the motile and sensory cilia which may be lost in the face of chemical exposure (70,

608 81, 82). We found marginally lower proportions of ciliated surface area on the olfactory
609 epithelium at the Calnali Low site (Mann-Whitney Test *P*-value = 0.08; Fig. 5C). Likewise,
610 AB/PAS staining clearly distinguished goblet cells through the deep blue staining of the
611 protective mucoproteins they produce, and revealed significantly higher densities of goblet cells
612 at Calnali Low (Mann-Whitney Test *P*-value = 0.002; Fig. 5D-F), consistent with a
613 compensatory response to shield the olfactory epithelium from toxicants.

614 **Discussion**

615

616 A more nuanced view of the genetic and environmental landscape of hybrid zones will
617 allow biologists to move past a binary picture of hybridization's presence or absence, and begin
618 to pinpoint the specific changes and mechanisms by which anthropogenic disturbance can drive
619 hybridization. By surveying genome-wide ancestry distributions at dozens of sites where *X.*
620 *birchmanni* and *X. malinche* coexist, we found that the patterns of hybridization varied
621 drastically within and between rivers. We detected some degree of gene flow between *X.*
622 *malinche* and *X. birchmanni* in all four rivers surveyed, but the amount and spatial distribution of
623 admixture differed across each river (Fig. 2, Supp. Info 9; Fig. S16-17). Thus, while there is
624 some potential for hybridization whenever related species overlap, the implications for
625 biodiversity are highly variable.

626 At one end of the spectrum of genetic homogenization, the Río Conzintla showed two
627 slightly admixed ancestry clusters which co-occur at multiple sites across 3.7 river kilometers,
628 resulting in a "bimodal" distribution of genome-wide ancestry at these sites. Within these sites,
629 individuals derived <15% of their genome-wide ancestry from the other species (mean ± SD
630 "minor" parent ancestry of 5.6 ± 3.1% at Xochicoatlán, 10.6 ± 4.5% at Mixtla). While this level
631 of admixture is evolutionarily significant, its functional consequences are likely limited by
632 genome-wide selection against introgression (49), and populations with similar admixture rates
633 have been designated as "conservation populations" in other cases of anthropogenic
634 hybridization (84). The stability of within-cluster admixture proportions across the entire length
635 of the Río Conzintla, combined with our observation of only 1 recent hybrid out of 239
636 individuals, suggests that gene flow between clusters in this river is extremely limited. The stable

hybrid zone in this stream thus serves as a contrast to other rivers, and comparisons in water quality may illuminate the potential drivers of breakdown in assortative mating in other contexts.

In contrast, the Huazalingo and Pochula rivers showed no sites with bimodal ancestry structure, but rather a sharp transition in genome-wide ancestry moving downstream. These rivers appear more similar to classic clinal hybrid zones, where ancestry patterns are shaped by the countervailing effects of gene flow and selection against hybrids (85). While the lack of any structured populations in these rivers prevented us from assessing the effects of environmental variation on rates of hybridization, we found that overall water chemistry in these rivers was quite similar to the Río Conzintla. We speculate that anthropogenic impacts may have played a role in the onset of hybridization in these rivers, but it is difficult to test such hypotheses in contemporary hybrid populations, since the weakening of mate preference in highly admixed individuals means that such clines could continue to exist even after environmental triggers disappear (86–88). These rivers nonetheless can provide important insights into the role of migration and ecological selection in structuring *X. malinche* × *X. birchmanni* hybrid zones (Supp. Info 9).

Lastly, the Río Calnali showed a dramatic change in ancestry structure from upstream to downstream. We observed strong bimodality in genome-wide ancestry at sites upstream of the town of Calnali, with individuals falling into one of two subpopulations, a *X. malinche*-like ancestry cluster and a *X. birchmanni*-like cluster. These results align with prior work documenting the presence of strong assortative mating by ancestry within *X. malinche* and *X. birchmanni*-like hybrid clusters at the Aguazarca site on the Río Calnali (Supp. Info 6) (55). Within a span of less than two river kilometers where the river traverses the town of Calnali, this bimodal population structure collapses into a hybrid swarm, with the range of observed

admixture proportions spanning the continuum between the upstream clusters (Fig. 2). The Río Calnali thus provides a powerful opportunity to study the environmental determinants of reproductive isolation through comparisons within and between rivers.

We took advantage of this remarkable system by measuring a large array of chemical parameters across rivers in parallel with our genomic surveys. In doing so, we identified substantial chemical variation both between rivers of the Atlapexco drainage and between sites upstream and downstream of the town of Calnali (Fig. 4). PCA highlighted river-specific water chemistry signatures, which we speculate may be driven by geology and the impacts of mining in the Conzintla drainage (see Supp. Info 3; Fig. S5). However, we also observe an independent chemical change among sites on the Río Calnali above and below the town of Calnali, while the other rivers were relatively stable in water chemistry along their lengths (Fig. 4). By quantifying land use across each drainage, we confirmed that the Calnali drainage is indeed unique both in the scale of built infrastructure relative to catchment area, as well as the proximity of development to the river (Fig. 3, Fig. S19). The clearing of forests for pasture and cropland could also contribute to the chemical disturbances we observe, but may be a less likely explanation given the relatively small differences in agricultural land areas within and between drainages (Fig. S20), as well as the low-intensity agricultural practices typical of the area (89, 90). Both agricultural and urban development have been linked to some of the changes in water chemistry that we observe in the downstream Río Calnali (91–95). In particular, many metals whose concentrations change along the course of the Calnali have been previously associated with both domestic wastewater and runoff from roads (93).

Among the many compounds which varied between rivers and disturbance regimes, a substantial number have been previously shown to affect olfaction in fishes (dissolved organic

683 matter, copper, aluminum, zinc (23, 96, 97)) or fish neurology more generally (ammonia, cobalt,
684 and cadmium (68, 74, 98)). Many of these parameters were specifically elevated in the Río
685 Calnali, and especially so in the areas downstream of the town. Thus, they are particularly
686 promising candidates for the drivers of ancestry structure breakdown. On the other hand, we
687 found that other ions with olfactory or neurological effects in the ecotoxicology literature
688 (manganese, arsenic, calcium (26, 99–101)) were most extreme in the Conzintla, where
689 reproductive isolation is maintained (Fig. S22, Fig. S24), suggesting that variation in these
690 specific parameters is not a primary driver of hybridization in *Xiphophorus*. Variation in pH
691 between streams may also play a role, as low pH increases metal bioavailability (Fig. S22; (96)).
692 Having established differences in both the degree of population structure and in water
693 chemistry between sites in the Río Calnali, we next explored the loss of olfaction-based
694 assortative mate preferences as a biological mechanism which might connect the two. Mother-
695 embryo sequencing and simulations demonstrate that assortative mating is substantially
696 weakened at downstream sites on the Río Calnali, but surprisingly, it is not entirely absent (Fig.
697 5B). Ongoing assortative mating could be driven by downstream migration, with mothers either
698 mating prior to migration, or retaining some ability to mate assortatively even after arriving in
699 highly polluted waters. Alternatively, weak assortative mating at the population scale could be
700 produced by differential vulnerability of various signal modalities to disturbance (e.g. visual vs.
701 olfactory cues, (102, 103)) or fluctuations in the degree of sensory disturbance fish experience as
702 a result of variation in environmental conditions (Supp. Info 4). Regardless of the mechanism,
703 this observation supports theoretical predictions that even a partial breakdown in assortative
704 mating may result in the emergence of hybrid swarms (28).

705 Finally, our histological sampling of fishes in the upstream and downstream Calnali shows
706 changes in cellular abundance and morphology consistent with olfactory damage. The loss of
707 cilia in the sensory epithelium has previously been observed after exposure to heavy metals and
708 anthropogenic hydrocarbons (78, 104), and could directly reduce olfactory sensitivity by
709 disrupting water flow through the nares (105, 106) or the function of olfactory sensory neurons
710 (107). Likewise, an increased number of goblet cells has been linked to inflammation secondary
711 to nasal irritation in other systems, and may be a protective response to noxious chemical
712 exposure (80, 83). These histological analyses represent the first evidence of higher olfactory
713 damage in a wild hybrid swarm relative to nearby structured populations. Whether these changes
714 themselves weaken assortative mating, or are correlated with other causative changes (e.g.
715 transport and accumulation of heavy metals in the brain's olfactory bulb (108)) is an exciting
716 direction for future work. While our results support the hypothesis that the breakdown of
717 assortative mating along the Río Calnali is mediated at least in part by olfactory dysfunction, our
718 short-term laboratory exposures of *X. birchmanni* to ecologically relevant levels of ammonia,
719 copper, humic acid, or their combination did not reproduce the effect (Fig. S15). The specific
720 chemical concentrations and exposure durations necessary to disrupt pre-mating isolation thus
721 remains a promising area for further study.
722 Taken as a whole, our study presents an integrative window into the environmental and
723 organismal drivers of hybridization between *X. birchmanni* and *X. malinche*. By showing that
724 dramatic water chemistry differences are tightly linked to changes in population structure, we
725 confirm the relevance of prior behavioral work showing the potential for changes in water
726 chemistry to disrupt assortative mating in these species (23, 26). Though many studies have
727 documented a connection between environmental conditions and hybridization in freshwater

728 fishes (3, 27), our analyses of assortative mating and olfactory histology provide a deeper
729 understanding of the proximal mechanisms by which water chemistry changes might disrupt
730 reproductive isolation. This multidimensional approach to the study of hybrid zones sheds light
731 on the routes by which anthropogenic change can impact biodiversity on small spatiotemporal
732 scales. As human impacts on the environment continue to expand, a greater understanding of the
733 drivers of hybridization will help to mitigate human impacts on biodiversity.

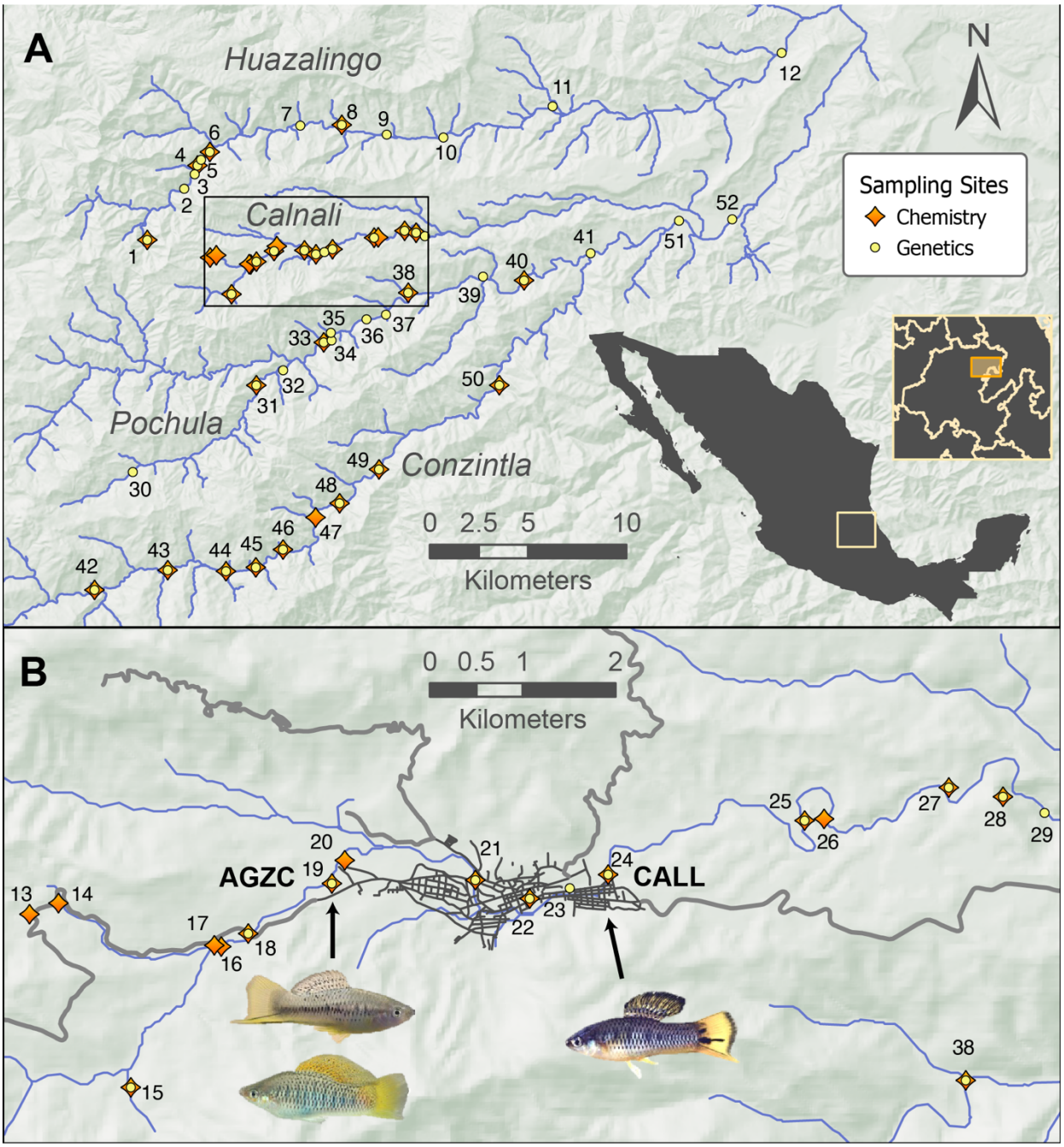

Figure 1. Study area and sampling sites. **A)** Overview of Río Atlapexco basin, highlighted in orange within the inset Mexican state map, whose area is indicated in yellow on the gray outline of Mexico. Rivers are shown as blue lines, the four major rivers studied are labelled, sites where fish were collected are yellow circles, and sites where water chemistry data were collected are orange diamonds. The black box encloses the area displayed in panel **B**. **B)** Sites sampled on Río

Calnali. Thick gray lines show major roadways, and thin black lines show streets in the town of Calnali. Images show representative male *Xiphophorus* fishes collected from two populations on the Río Calnali (AGZC = Aguazarca, CALL = Calnali Low). These sites were also the locations used for sample collection for histology. In the Río Calnali, *X. malinche*-like fish are found in the headwaters, *X. malinche*-like and *X. birchmanni*-like fishes are found upstream of the town of Calnali, and fish with intermediate genotypes and phenotypes are found downstream of town.

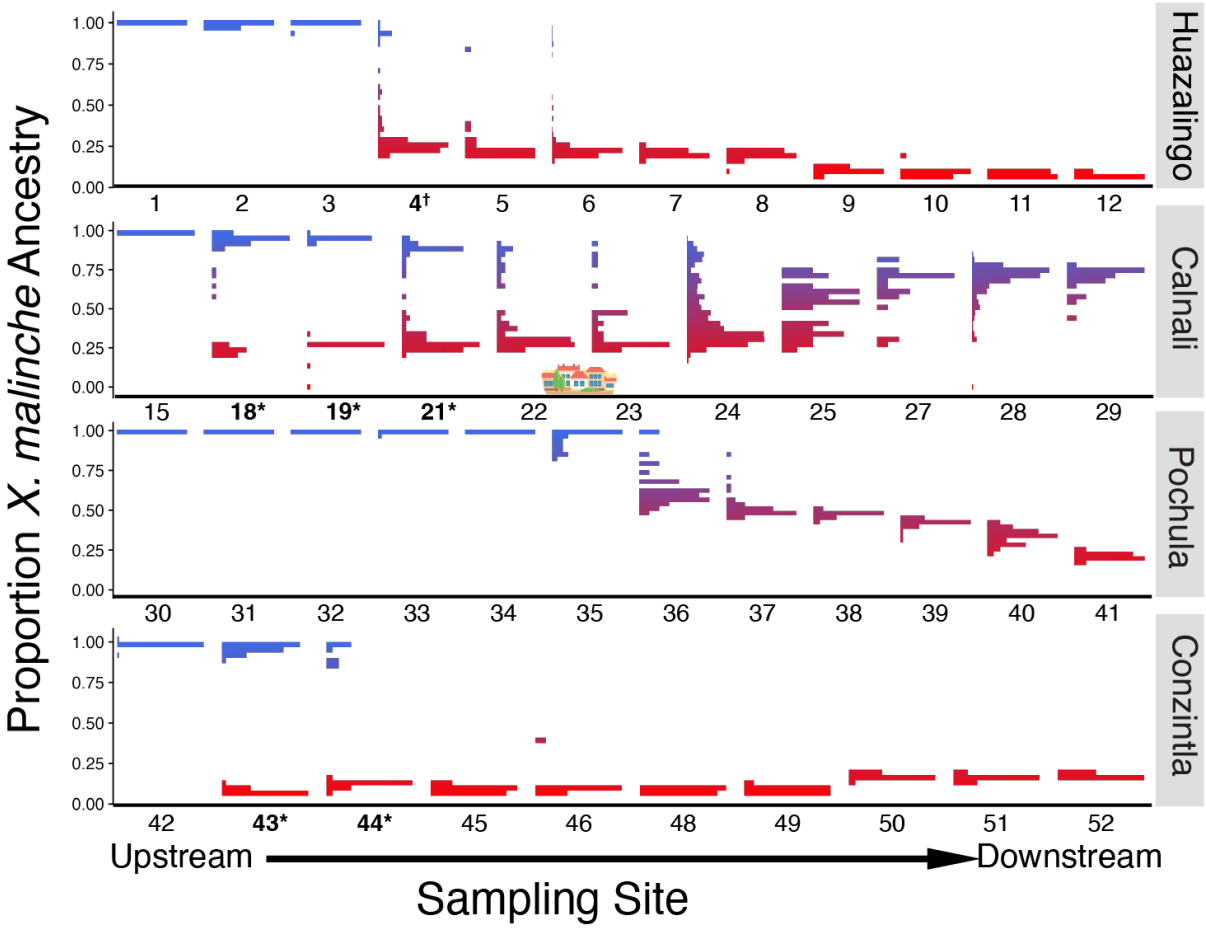

Figure 2. Genetic ancestry results from *X. malinche* × *X. birchmanni* hybrids in the Río Atlapexco Drainage. Histograms show ancestry distributions at sampling locations along four rivers in the Río Atlapexco drainage. Sites are arranged with upstream sites on the left side of the X-axis, and downstream sites on the right. Y-axis corresponds to the proportion of genome-wide ancestry derived from *X. malinche* among individuals in that populations (1 = pure *X. malinche*, 0 = pure *X. birchmanni*), and the width of bars indicates the frequency of individuals in that ancestry bin. Building icon on the Río Calnali transect denotes the sites located within the town of Calnali. X-axis text shows site numbers, as in Fig. 1. Bolded X-axis numbers indicate sites with significant deviations from a unimodal ancestry distribution, either across all sampling timepoints (asterisk) or at a subset of sampling times (dagger, Supp. Info. 2).

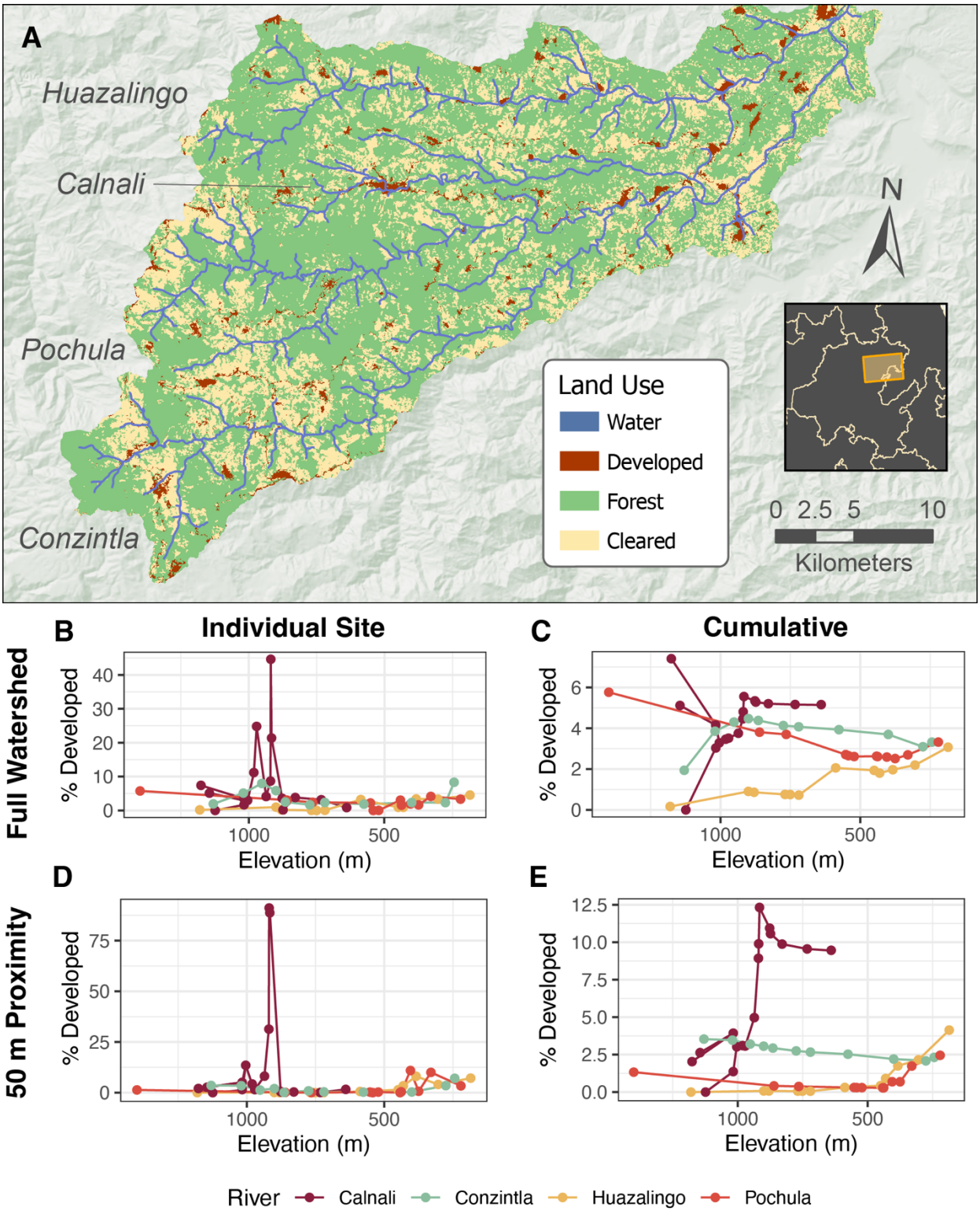

Figure 3. Results of land use classification analysis in the Río Atlapexco basin. **A**) Map of classification results from 2020-2023 hyperspectral imagery. 10 m^2 pixels were classified as

developed (buildings, mines, and roads), cleared land (grassland, pasture, or cultivated crops) forest (continuous tree cover, excluding plantation-style agriculture), or water by an SVM algorithm, with training polygons identified from 3 m^2-resolution 2022 imagery from Planet Labs (61). River polygons are shown as blue lines over classified pixels. **B-E)** Percent of land classified as developed within different drainages of the Río Atlapexco basin. Points show the proportion of pixels in each site's subcatchment that were classified as developed. Left column (**B** and **D**) shows the site-wise proportions, or the subcatchment of the section of river between a site and the closest upstream site. Right column (**C** and **E**) shows the cumulative subcatchment of all sections of the river upstream of a given site. Top row (**B** and **C**) shows calculations that include pixels of any distance from a stream, while bottom row (**D** and **E**) shows calculations limited to pixels within 50 m of a stream (defined as pixels with accumulated flow > 3000 cells, depicted with river polygons in **A**). Color denotes the drainage that the site occurs in, and lines connect sites in the same river based on their order. The line corresponding to the Río Calnali branches because multiple headwater tributaries were sampled.

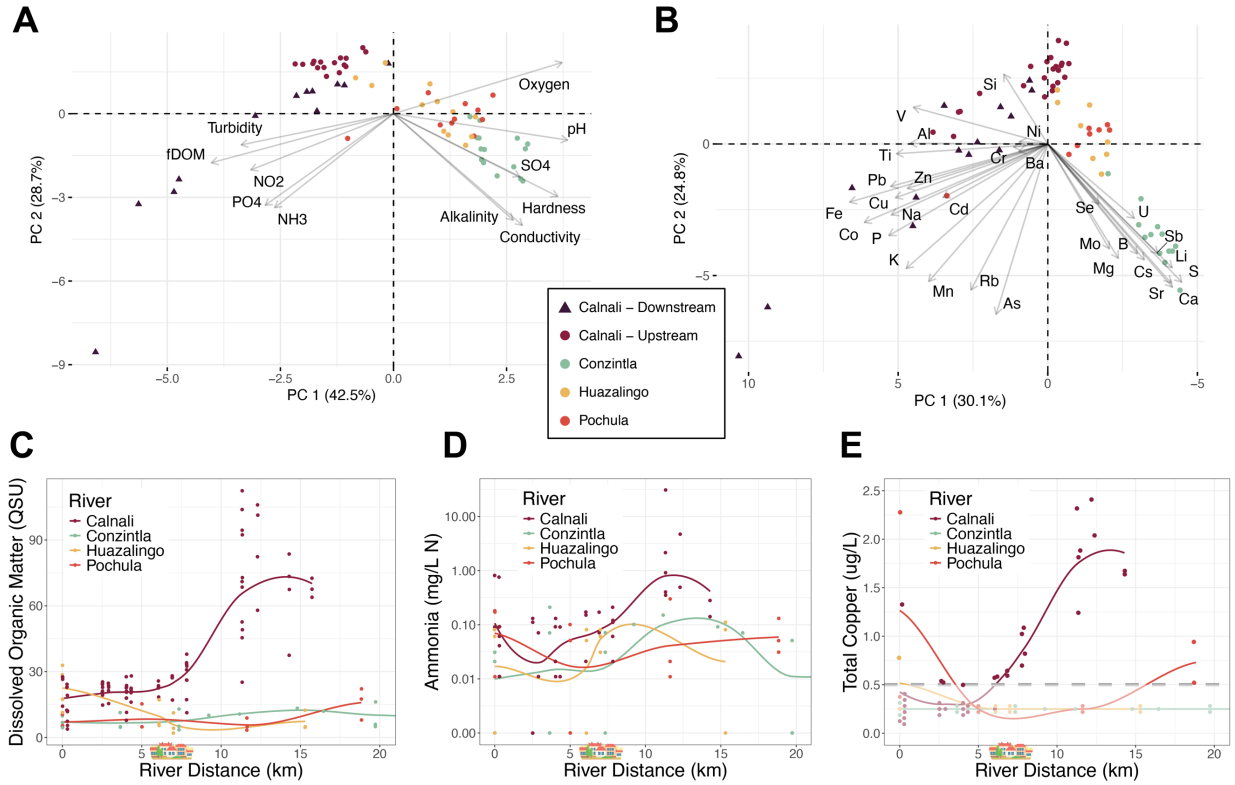

Figure 4. Water chemistry data from four rivers in the Río Atlapexco drainage. **A-B)** Principal component analysis (PCA) biplot for **A)** parameters measured using the sonde, turbidimeter, colorimeter, and **B)** parameters measured using ICP-MS. Points represent sampling events, and color and shape denote drainage, with sites on the Río Calnali upstream and downstream of the town of Calnali labelled separately. Labelled arrows represent variable loadings onto first two principal components, with highly correlated variables showing similar vectors. **C-E)** Plots of the change in water chemistry over the course of the river, focusing on parameters that were elevated in sites downstream of the town of Calnali. These include **C)** fluorescent dissolved organic matter, **D)** ammonia, and **E)** total copper. The building icon on the X-axis denotes the sites located within the town of Calnali on the Río Calnali transect. X-axis indicates distance downstream from the first site sampled on a river, points indicate individual measurements, and lines show a loess-spline fit of change over the river course. Note that the Y-axis is log-scaled in

the case of ammonia measurements (**D**). Translucent points below the gray dashed line in **E)** represent measured values below the detection limit of the ICP-MS assay. Points below this limit are plotted at half the detection threshold, with jittering to prevent overlap and represent sample size, but do not represent point estimates of the concentration.

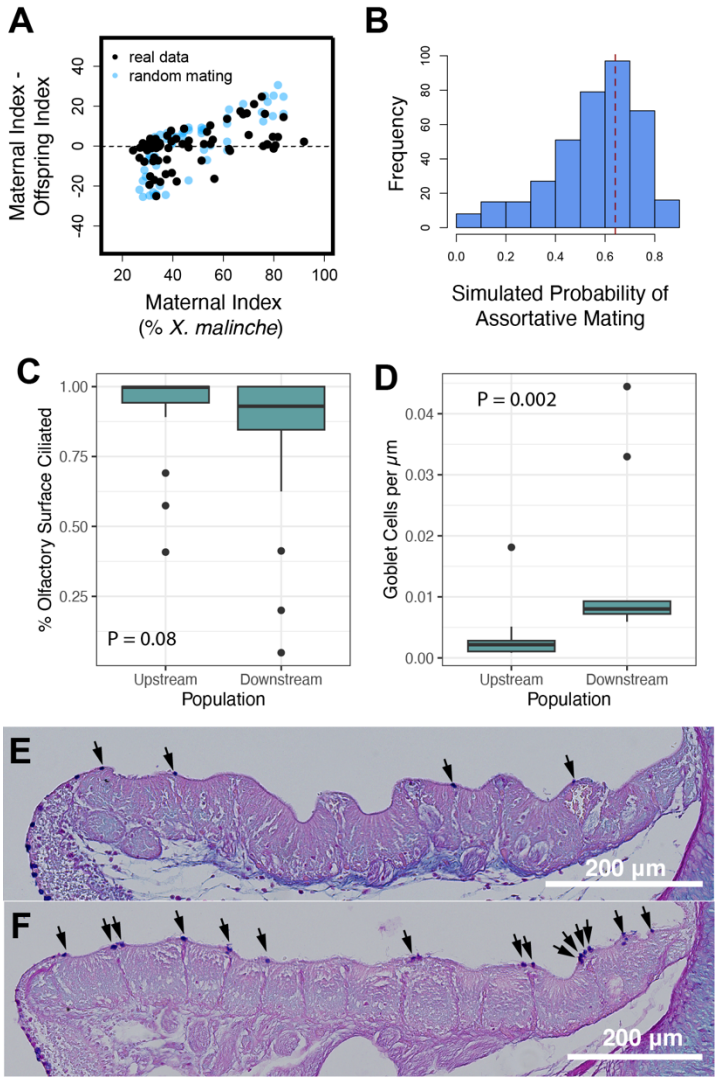

Figure 5. Mating patterns and histological phenotypes in fishes upstream and downstream of the town of Calnali. **A)** Results of mother-embryo sequencing analysis based on individuals collected at the Calnali Low site, downstream of the town of Calnali. X-axis shows the proportion of each mother's genome derived from *X. malinche*, and Y-axis shows the difference in genome-wide *X. malinche* ancestry between each mother and embryo. Mean maternal-offspring ancestry difference was significantly but modestly lower in real data (black) than in simulated data modeling random mating (blue; $P < 0.001$ by simulation). **B)** Inferred strength of assortative mating from observed maternal-offspring ancestry distributions. Blue bars depict the

simulated probability of assortative mating in accepted simulations, with 0 representing random mating. Dashed line denotes maximum a posteriori estimate ($P_{assortative}$ = 0.65). **C-D)** Results of olfactory histology of fishes from sites upstream (Aguazarca) and downstream (Calnali Low) of the town of Calnali. **C)** Proportion of each fish's sensory epithelium with visible cilia, visualized with H&E staining. **D)** Number of mucus-producing goblet cells per µm of olfactory rosette surface area, visualized by staining with AB/PAS. *P*-values indicate results of Mann-Whitney *U* Test for difference between sites. **E-F)** Representative AB/PAS stains of olfactory rosettes of *X. malinche* × *birchmanni* hybrids from **E)** Aguazarca, and **F)** Calnali Low. Mucoproteins are stained blue by AB/PAS, eosin counterstain appears as pink. Arrowheads indicate locations of goblet cells.

Acknowledgements

The authors thank members of the Schumer and Rosenthal laboratories for helpful discussion and/or feedback on earlier versions of this manuscript. We thank the Federal Government of Mexico for permission to collect fish (Permiso de Pesca de Fomento no. PPF/DGOPA-064/20). Stanford University and the Stanford Research Computing Center provided computational support for this project. We thank Dra. Susana Saval Bohórquez of the UNAM Environmental Engineering Laboratory and Dr. Guangchao Li and Douglas Turner of the Stanford Environmental Measurements Facility for technical and experimental support. This work was supported by a Knight–Hennessy Scholars fellowship and NSF GRFP 2019273798 to B.M.M., a CONACyT fellowship to GIJ, NSF Awards 1723266, 1755327 and 1354172 to GGR, and Human Frontiers in Science Grant RGY0081 to MS & CMR.

References

1. E. Mayr, *Systematics and the Origin of Species: from the Viewpoint of a Zoologist* (Columbia University Press, 1942).

2. E. Anderson, Hybridization of the habitat. *Evolution* 1–9 (1948).

3. K. C. Grabenstein, S. A. Taylor, Breaking Barriers: Causes, Consequences, and Experimental Utility of Human-Mediated Hybridization. *Trends in Ecology & Evolution* **33**, 198–212 (2018).

4. R. Ubsdell, Studies on variation and evolution in Centaurium erythraea Rafn and C. littorale (D. Turner) Gilmour in the British Isles. 3. Breeding systems, floral biology and general discussion. *Watsonia* **12**, 225–232 (1979).

5. C. Brochmann, Hybridization and distribution of Argyranthemum coronopifolium (Asteraceae – Anthemideae) in the Canary Islands. *Nordic Journal of Botany* **4**, 729–736 (1984).

6. O. Seehausen, J. J. M. van Alphen, F. Witte, Cichlid Fish Diversity Threatened by Eutrophication That Curbs Sexual Selection. *Science* **277**, 1808–1811 (1997).

7. P. Vonlanthen, *et al.*, Eutrophication causes speciation reversal in whitefish adaptive radiations. *Nature* **482**, 357–362 (2012).

8. E. C. Ellis, Anthropogenic transformation of the terrestrial biosphere. *Philosophical Transactions of the Royal Society A: Mathematical, Physical and Engineering Sciences* **369**, 1010–1035 (2011).

9. J. A. Coyne, H. A. Orr, *Speciation* (Sinauer Associates, 2004).

10. D. A. Turissini, J. A. McGirr, S. S. Patel, J. R. David, D. R. Matute, The Rate of Evolution of Postmating-Prezygotic Reproductive Isolation in Drosophila. *Molecular Biology and Evolution* **35**, 312–334 (2018).

11. D. I. Bolnick, T. J. Near, Tempo of Hybrid Inviability in Centrarchid Fishes (TELeostei: Centrarchidae). *Evolution* **59**, 1754–1767 (2005).

12. C. E. Wagner, L. J. Harmon, O. Seehausen, Ecological opportunity and sexual selection together predict adaptive radiation. *Nature* **487**, 366–369 (2012).

13. O. Puebla, E. Bermingham, F. Guichard, Pairing dynamics and the origin of species. *Proceedings of the Royal Society of London B: Biological Sciences* **279**, 1085–1092 (2012).

14. J.-G. J. Godin, S. E. Briggs, Female mate choice under predation risk in the guppy. *Animal Behaviour* **51**, 117–130 (1996).

15. P. M. Willis, M. J. Ryan, G. G. Rosenthal, Encounter rates with conspecific males influence female mate choice in a naturally hybridizing fish. *Behavioral Ecology* **22**, 1234–1240 (2011).

16. M. N. Verzijden, Z. W. Culumber, G. G. Rosenthal, Opposite effects of learning cause asymmetric mate preferences in hybridizing species. *Behavioral Ecology* **23**, 1133–1139 (2012).

17. J. Hunt, R. Brooks, M. D. Jennions, Female Mate Choice as a Condition-Dependent Life-History Trait. *The American Naturalist* **166**, 79–92 (2005).

18. A. E. Hausmann, *et al.*, Light environment influences mating behaviours during the early stages of divergence in tropical butterflies. *Proceedings of the Royal Society B: Biological Sciences* **288**, 20210157 (2021).

19. K. S. Pfennig, Facultative mate choice drives adaptive hybridization. *Science* **318**, 965–967 (2007).

20. G. G. Rosenthal, D. Stuart-Fox, others, "Environmental disturbance and animal communication" in *Behavioural Responses to a Changing World: Mechanisms and Consequences*, (Oxford University Press, 2015), pp. 16–31.

21. G. G. Rosenthal, Individual mating decisions and hybridization. *Journal of Evolutionary Biology* **26**, 252–255 (2013).

22. B. Seifert, J. Kulmuni, P. Pamilo, Independent hybrid populations of Formica polyctena Xrufa wood ants (Hymenoptera: Formicidae) abound under conditions of forest fragmentation. *Evol Ecol* **24**, 1219–1237 (2010).

23. H. S. Fisher, B. B. M. Wong, G. G. Rosenthal, Alteration of the chemical environment disrupts communication in a freshwater fish. *Proc R Soc B* **273**, 1187–1193 (2006).

24. J. L. Ward, M. J. Blum, Exposure to an environmental estrogen breaks down sexual isolation between native and invasive species. *Evolutionary Applications* **5**, 901–912 (2012).

25. P. C. Hubbard, E. N. Barata, A. V. M. Canario, Possible disruption of pheromonal communication by humic acid in the goldfish, Carassius auratus. *Aquatic Toxicology* **60**, 169–183 (2002).

26. D. L. Powell, A. D. Rose, G. G. Rosenthal, A widely-used pollutant causes reversal of conspecific mate preference in a freshwater fish. [Preprint] (2022). Available at: https://www.biorxiv.org/content/10.1101/2022.09.07.507014v1 [Accessed 2 September 2023].

27. W. F. Ramirez-Duarte, *et al.*, Hybridization in the Anthropocene – how pollution and climate change disrupt mate selection in freshwater fish. *Biological Reviews* **0** (2024).

28. R. T. Gilman, J. E. Behm, Hybridization, Species Collapse, and Species Reemergence After Disturbance to Premating Mechanisms of Reproductive Isolation. *Evolution* **65**, 2592–2605 (2011).

29. D. J. Hasselman, *et al.*, Human disturbance causes the formation of a hybrid swarm between two naturally sympatric fish species. *Molecular Ecology* **23**, 1137–1152 (2014).

30. T. B. Malek, J. W. Boughman, I. Dworkin, C. L. Peichel, Admixture mapping of male nuptial colour and body shape in a recently formed hybrid population of threespine stickleback. *Molecular Ecology* **21**, 5265–5279 (2012).

31. B. Alric, *et al.*, Local human pressures influence gene flow in a hybridizing Daphnia species complex. *Journal of Evolutionary Biology* **29**, 720–735 (2016).

32. T. van Hengstum, *et al.*, Human-induced hybridization among congeneric endemic plants on Tenerife, Canary Islands. *Plant Syst Evol* **298**, 1119–1131 (2012).

33. J. I. Meier, *et al.*, Ancient hybridization fuels rapid cichlid fish adaptive radiations. *Nature Communications* **8**, 14363 (2017).

34. S. A. Taylor, E. L. Larson, Insights from genomes into the evolutionary importance and prevalence of hybridization in nature. *Nat Ecol Evol* **3**, 170–177 (2019).

35. R. J. Abbott, N. H. Barton, J. M. Good, Genomics of hybridization and its evolutionary consequences. *Molecular Ecology* **25**, 2325–2332 (2016).

36. M. Schumer, R. Cui, G. G. Rosenthal, P. Andolfatto, Reproductive Isolation of Hybrid Populations Driven by Genetic Incompatibilities. *PLoS Genet* **11**, e1005041 (2015).

37. C. Veller, N. B. Edelman, P. Muralidhar, M. A. Nowak, Recombination and selection against introgressed DNA. *Evolution* **77**, 1131–1144 (2023).

38. C. Chen, K. S. Pfennig, Female toads engaging in adaptive hybridization prefer high-quality heterospecifics as mates. *Science* **367**, 1377–1379 (2020).

39. N. B. Edelman, J. Mallet, Prevalence and Adaptive Impact of Introgression. *Annu Rev Genet* **55**, 265–283 (2021).

40. M. Ribeiro Palacios, Land use change in Southern Huasteca, Mexico; drivers and consequences for livelihood and ecosystem services. (2012).

41. H. R. Hernández, M. A. Robledo, J. R. A. Rivera, J. F. Martinez, Spatial Configuration of Land-Use/Land-Cover in the Pujal-Coy Project Area, Huasteca Potosina Region, Mexico. *Ambio* **37**, 381–389 (2008).

42. M. L. Martínez, *et al.*, Effects of land use change on biodiversity and ecosystem services in tropical montane cloud forests of Mexico. *Forest Ecology and management* **258**, 1856–1863 (2009).

43. L. Chapa-Vargas, K. Monzalvo-Santos, Natural protected areas of San Luis Potosí, Mexico: ecological representativeness, risks, and conservation implications across scales. *International Journal of Geographical Information Science* **26**, 1625–1641 (2012).

44. C. Payne, *et al.*, Genomic insights into variation in thermotolerance between hybridizing swordtail fishes. *Mol Ecol* (2022). https://doi.org/10.1111/mec.16489.

45. Z. W. Culumber, D. B. Shepard, S. W. Coleman, G. G. Rosenthal, M. Tobler, Physiological adaptation along environmental gradients and replicated hybrid zone structure in swordtails (Teleostei: Xiphophorus). *Journal of Evolutionary Biology* **25**, 1800–1814 (2012).

46. D. L. Powell, *et al.*, Natural hybridization reveals incompatible alleles that cause melanoma in swordtail fish. *Science* **368**, 731–736 (2020).

47. B. M. Moran, *et al.*, A lethal mitonuclear incompatibility in complex I of natural hybrids. *Nature* **626**, 119–127 (2024).

48. M. Schumer, Y. Brandvain, Determining epistatic selection in admixed populations. *Mol Ecol* **25**, 2577–2591 (2016).

49. M. Schumer, *et al.*, Natural selection interacts with recombination to shape the evolution of hybrid genomes. *Science* **360**, 656–660 (2018).

50. Z. W. Culumber, *et al.*, Replicated hybrid zones of *Xiphophorus* swordtails along an elevational gradient. *Mol Ecol* **20**, 342–356 (2011).

51. M. Rauchenberger, I. K. D. Kallman, Monophyly and Geography of the Rio P'anuco Basin Swordtails (Genus Xiphophorus) with Descriptions of Four New Species. *AMERICAN MUSEUM NOVITATES* 44 (1990).

52. G. G. Rosenthal, *et al.*, Dissolution of Sexual Signal Complexes in a Hybrid Zone between the Swordtails Xiphophorus birchmanni and Xiphophorus malinche (Poeciliidae). *Copeia* **2003**, 299–307 (2003).

53. INEGI, México en cifras. (1998). Available at: https://www.inegi.org.mx/app/areasgeograficas/ [Accessed 6 April 2025].

54. M. Schumer, *et al.*, High-resolution mapping reveals hundreds of genetic incompatibilities in hybridizing fish species. *eLife* **3**, e02535 (2014).

55. M. Schumer, *et al.*, Assortative mating and persistent reproductive isolation in hybrids. *Proc Natl Acad Sci USA* **114**, 10936–10941 (2017).

56. M. Schumer, D. L. Powell, R. Corbett-Detig, Versatile simulations of admixture and accurate local ancestry inference with mixnmatch and ancestryinfer. *Molecular Ecology Resources* **20**, 1141–1151 (2020).

57. S. M. Banerjee, *et al.*, Complex hybridization between deeply diverged fish species in a disturbed ecosystem. *Evolution* **77**, 995–1005 (2023).

58. J. A. Hartigan, P. M. Hartigan, The Dip Test of Unimodality. *The Annals of Statistics* **13**, 70–84 (1985).

59. European Union/ESA/Copernicus, Sentinel-2 MSI: MultiSpectral Instrument, Level-2A. (2020).

60. J. Transon, R. D'Andrimont, A. Maugnard, P. Defourny, Survey of Hyperspectral Earth Observation Applications from Space in the Sentinel-2 Context. *Remote Sensing* **10**, 157 (2018).

61. Planet Labs, Planetscope Scene, March 29 2022, Instrument PS2.SD, Strip 5529184. (2022).

62. INEGI, Continuo de elevaciones mexicano y modelos digitales de elevación v3. (2013).

63. A. Kamal, K. Wichuk, D. McCartney, K. Londry, C. Felske, Effect of Treated Wood on Biosolids Composting. *Compost Science & Utilization* **25**, 178–193 (2017).

64. K. J. Pieper, *et al.*, Evaluating Water Lead Levels During the Flint Water Crisis. *Environ. Sci. Technol.* **52**, 8124–8132 (2018).

65. D. R. Helsel, *Nondetects and data analysis. Statistics for censored environmental data.* (2005).

66. O. Seehausen, *et al.*, Speciation through sensory drive in cichlid fish. *Nature* **455**, 620–626 (2008).

67. J.-H. Kim, S. K. Kim, Y. B. Hur, Toxic effects of waterborne nitrite exposure on antioxidant responses, acetylcholinesterase inhibition, and immune responses in olive flounders, *Paralichthys olivaceus*, reared in bio-floc and seawater. *Fish & Shellfish Immunology* **97**, 581–586 (2020).

68. Y. K. Ip, S. F. Chew, D. J. Randall, “Ammonia toxicity, tolerance, and excretion” in *Fish Physiology*, Nitrogen Excretion., (Academic Press, 2001), pp. 109–148.

69. D. J. Randall, T. K. N. Tsui, Ammonia toxicity in fish. *Marine Pollution Bulletin* **45**, 17–23 (2002).

70. J. A. Hansen, J. D. Rose, R. A. Jenkins, K. G. Gerow, H. L. Bergman, Chinook salmon (Oncorhynchus tshawytscha) and rainbow trout (Oncorhynchus mykiss) exposed to copper: Neurophysiological and histological effects on the olfactory system. *Environmental Toxicology and Chemistry* **18**, 1979–1991 (1999).

71. W. A. Dew, A. Azizishirazi, G. G. Pyle, Contaminant-specific targeting of olfactory sensory neuron classes: Connecting neuron class impairment with behavioural deficits. *Chemosphere* **112**, 519–525 (2014).

72. J.-W. Lee, *et al.*, Toxic effects of lead exposure on bioaccumulation, oxidative stress, neurotoxicity, and immune responses in fish: A review. *Environmental Toxicology and Pharmacology* **68**, 101–108 (2019).

73. C. R. Williams, E. P. Gallagher, Effects of cadmium on olfactory mediated behaviors and molecular biomarkers in coho salmon (Oncorhynchus kisutch). *Aquatic Toxicology* **140–141**, 295–302 (2013).

74. K. Heffern, K. Tierney, E. P. Gallagher, Comparative effects of cadmium, zinc, arsenic and chromium on olfactory-mediated neurobehavior and gene expression in larval zebrafish (*Danio rerio*). *Aquatic Toxicology* **201**, 83–90 (2018).

75. J. T. Hentig, C. A. Byrd-Jacobs, Exposure to zinc sulfate results in differential effects on olfactory sensory neuron subtypes in adult zebrafish. *International journal of molecular sciences* **17**, 1445 (2016).

76. D. A. Klaprat, S. Brown, T. J. Hara, The effect of low pH and aluminum on the olfactory organ of rainbow trout, Salmo gairdneri. *Environmental Biology of Fishes* **22**, 69–77 (1988).

77. E. Zeiske, R. Melinkat, H. Breucker, J. Kux, Ultrastructural studies on the epithelia of the olfactory organ of cyprinodonts (teleostei, cyprinodontoidea). *Cell Tissue Res.* **172**, 245–267 (1976).

78. P. A. Triana-Garcia, "Studies on The Olfactory Biology and Behavioral Responses to Copper Exposure of The Native Indicator Species Delta Smelt (Hypomesus transpacificus)," UC Davis. (2021).

79. P. A. Triana-Garcia, G. A. Nevitt, J. B. Pesavento, S. J. Teh, Gross morphology, histology, and ultrastructure of the olfactory rosette of a critically endangered indicator species, the Delta Smelt, Hypomesus transpacificus. *J Comp Physiol A Neuroethol Sens Neural Behav Physiol* **207**, 597–616 (2021).

80. T. Shimizu, "Mucus, Goblet Cell, Submucosal Gland" in *Nasal Physiology and Pathophysiology of Nasal Disorders*, T. M. Önerci, Ed. (Springer, 2013), pp. 1–14.

81. M. Lazzari, S. Bettini, L. Milani, M. G. Maurizii, V. Franceschini, Differential response of olfactory sensory neuron populations to copper ion exposure in zebrafish. *Aquatic Toxicology* **183**, 54–62 (2017).

82. K. E. Klima, F. M. Applehans, Copper exposure and the degeneration of olfactory receptors in rainbow trout (Oncorhynchus mykiss). *Chemical Speciation & Bioavailability* **2**, 149–154 (1990).

83. D. Saucier, L. Astic, Morpho-functional alterations in the olfactory system of rainbow trout (*Oncorhynchus mykiss*) and possible acclimation in response to long-lasting exposure to low copper levels. *Comparative Biochemistry and Physiology Part A: Physiology* **112**, 273–284 (1995).

84. Fish and Wildlife Service, US Department of the Interior, Endangered and Threatened Wildlife and Plants; 90-Day Finding on a Petition To List the Colorado River Cutthroat Trout. *Federal Register* **69**, 21151–21158 (2004).

85. N. H. Barton, K. S. Gale, "Genetic Analysis of Hybrid Zones" in *Hybrid Zones and the Evolutionary Process*, p. 33.

86. B.-J. Velthuis, W. Yang, T. Van Opijnen, J. H. Werren, Genetics of female mate discrimination of heterospecific males in *Nasonia* (Hymenoptera, Pteromalidae). *Animal Behaviour* **69**, 1107–1120 (2005).

87. O. Svensson, *et al.*, The genetics of mate preferences in hybrids between two young and sympatric Lake Victoria cichlid species. *Proceedings of the Royal Society B: Biological Sciences* **284**, 20162332 (2017).

88. E. M. Schmidt, K. S. Pfennig, Hybrid female mate choice as a species isolating mechanism: environment matters. *Journal of Evolutionary Biology* **29**, 865–869 (2016).

89. R. M. Paulette, Uno de los rostros de la migración interna. Marginación y pobreza en la sierra hidalguense. *Sociológica México* 157–191 (2015).

90. S. Cruz Hernández, *et al.*, Saberes tradicionales locales y el cambio climático global. *Revista mexicana de ciencias agrícolas* **11**, 1917–1928 (2020).

91. Y. Xia, C. Ti, D. She, X. Yan, Linking river nutrient concentrations to land use and rainfall in a paddy agriculture–urban area gradient watershed in southeast China. *Science of The Total Environment* **566–567**, 1094–1105 (2016).

92. E. Apeagyei, M. S. Bank, J. D. Spengler, Distribution of heavy metals in road dust along an urban-rural gradient in Massachusetts. *Atmospheric Environment* **45**, 2310–2323 (2011).

93. J. J. Sansalone, J. P. Hird, F. K. Cartledge, M. E. Tittlebaum, Event-Based Stormwater Quality and Quantity Loadings from Elevated Urban Infrastructure Affected by Transportation. *Water Environment Research* **77**, 348–365 (2005).

94. S. Yu, *et al.*, Anthropogenic land uses elevate metal levels in stream water in an urbanizing watershed. *Science of The Total Environment* **488–489**, 61–69 (2014).

95. V. Paul, M. S. Sankar, S. Vattikuti, P. Dash, Z. Arslan, Pollution assessment and land use land cover influence on trace metal distribution in sediments from five aquatic systems in southern USA. *Chemosphere* **263**, 128243 (2021).

96. D. H. Baldwin, C. P. Tatara, N. L. Scholz, Copper-induced olfactory toxicity in salmon and steelhead: Extrapolation across species and rearing environments. *Aquatic Toxicology* **101**, 295–297 (2011).

97. A. E. Smith, “The influence of sub-lethal zinc exposure on olfaction of alarm cues and associated alarm behaviours in juvenile coho salmon,” University of British Columbia. (2023).

98. L. Sonnack, *et al.*, Effects of metal exposure on motor neuron development, neuromasts and the escape response of zebrafish embryos. *Neurotoxicology and Teratology* **50**, 33–42 (2015).

99. H. Tjälve, C. Mejàre, K. Borg-Neczak, Uptake and Transport of Manganese in Primary and Secondary Olfactory Neurones in Pike. *Pharmacology & Toxicology* **77**, 23–31 (1995).

100. Y. Rodríguez-Agudelo, *et al.*, Motor alterations associated with exposure to manganese in the environment in Mexico. *Science of The Total Environment* **368**, 542–556 (2006).

101. D. B. Szymkowicz, *et al.*, Exposure to arsenic during embryogenesis impairs olfactory sensory neuron differentiation and function into adulthood. *Toxicology* **420**, 73–84 (2019).

102. J. Lunt, D. L. Smee, Turbidity interferes with foraging success of visual but not chemosensory predators. *PeerJ* **3**, e1212 (2015).

103. S. M. Leahy, M. I. McCormick, M. D. Mitchell, M. C. O. Ferrari, To fear or to feed: the effects of turbidity on perception of risk by a marine fish. *Biology Letters* **7**, 811–813 (2011).

104. S. J. Song, B. Park, K. Jo, C.-S. Kim, Damage to Olfactory Organs of Adult Zebrafish Induced by Diesel Particulate Matter. *International Journal of Molecular Sciences* **23**, 407 (2022).

105. I. Reiten, *et al.*, Motile-Cilia-Mediated Flow Improves Sensitivity and Temporal Resolution of Olfactory Computations. *Current Biology* **27**, 166–174 (2017).

106. J. P. L. Cox, Hydrodynamic aspects of fish olfaction. *Journal of The Royal Society Interface* **5**, 575–593 (2008).

107. D. P. McEwen, P. M. Jenkins, J. R. Martens, "Chapter 12 Olfactory Cilia: Our Direct Neuronal Connection to the External World" in *Current Topics in Developmental Biology*, Ciliary Function in Mammalian Development., (Academic Press, 2008), pp. 333–370.

108. F. W. Sunderman, Nasal Toxicity, Carcinogenicity, and Olfactory Uptake of Metals. *Ann Clin Lab Sci* **31**, 3–24 (2001).